

Highlights

Encoder-Inverter Framework for Seismic Acoustic Impedance Inversion

Junheng Peng, Yingtian Liu, Mingwei Wang, Yong Li, Wen Feng

- We propose a new seismic acoustic impedance inversion workflow based on feature extraction and fine-tuning
- By mapping seismic traces into linear features, we can effectively address the problem of acoustic impedance inversion with limited well-logging data
- The method we proposed can achieve better performance and robustness than previous methods

Encoder-Inverter Framework for Seismic Acoustic Impedance Inversion

Junheng Peng^{a,b}, Yingtian Liu^{a,b}, Mingwei Wang^{a,b}, Yong Li^{a,b}, Wen Feng^b

^aThe Key Laboratory of Earth Exploration & Information Techniques of Ministry Education, Chengdu University of Technology, Chengdu, 610059, Sichuan, China

^bSchool of Geophysics, Chengdu University of Technology, Chengdu, 610059, Sichuan, China

Abstract

Seismic acoustic impedance inversion is one of the most challenging tasks in geophysical exploration, facing difficulties such as insufficient well-logging data and non-linear relationships. Most inversion methods rely on strategies such as semi-supervised learning, and their inversion accuracy and stability still need further improvement. In this work, we propose a novel inversion framework that innovatively maps continuous seismic traces into high-dimensional linear features, transforming the entire inversion task into a linear extrapolation or interpolation problem to improve inversion stability. To achieve this goal, we designed two auxiliary networks to train the encoder. Meanwhile, the model adopts a heterogeneous structure to avoid shortcut learning, so as to extract more generalized and effective linear features. We tested our method on the most widely used datasets, and the experiments show that compared with some previous methods, the proposed method achieves higher inversion accuracy and stability. Finally, to ensure the reproducibility of the experiments, we will open-source the data and code.

Keywords: Acoustic impedance inversion, Seismic signal processing, Feature exaction, Fine-tuning, Few-shot learning

1. Introduction

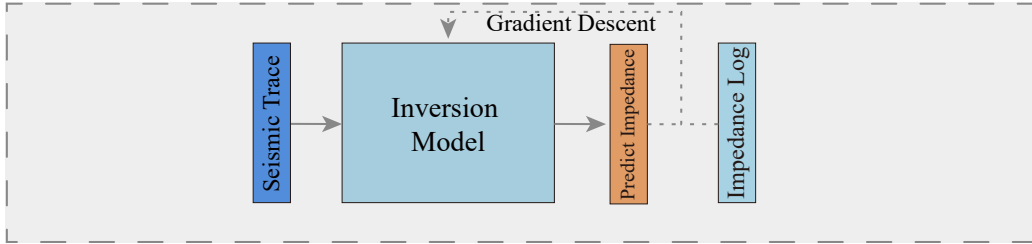
Seismic acoustic impedance inversion (AII) is a very important but challenging task in geophysical exploration, which performs imaging of subsurface lithology and structural changes through seismic data and a small amount of well-logging data (Doyen, 2007) (Lin et al., 2023). However, limited by

exploration costs, data (especially well data) are often scarce, which makes the AII problem ill-posed (Tamaddon-Jahromi et al., 2020).

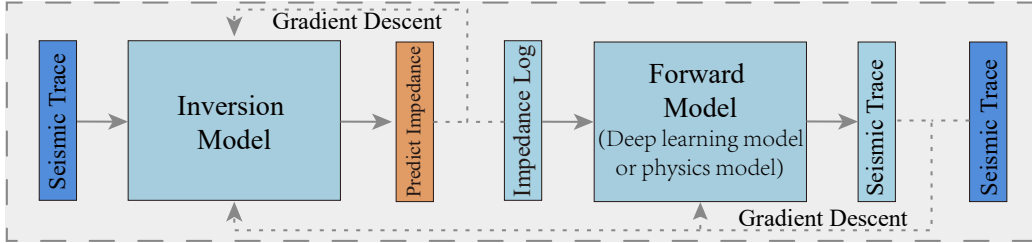
Initially, many researchers used optimization methods to carry out AII work. These optimization methods mainly include: least squares method (Lines and Treitel, 1984), simulated annealing (Srivastava and Sen, 2009), ant colony algorithm (Conti et al., 2013), genetic algorithm (Mallick, 1995), and particle swarm optimization (Shaw and Srivastava, 2007). Over the past few decades, these optimization methods have matured (de Figueiredo et al., 2017) (Zhao et al., 2025), yet the problems they still cannot solve include: firstly, the performance of these methods depends on the initial model (Yuan et al., 2019), but obtaining a good initial model is very difficult; secondly, these methods require an accurate seismic wavelet, thus relying on seismic wavelet extraction; thirdly, those methods generally have low computational efficiency; finally, various optimization methods lack prior information, and the use of manually designed regularization terms (such as $L1$ and L_p norm) makes it difficult to effectively reflect subsurface medium information.

With the development of computer technology, various deep learning (DL) methods have provided new solutions for data processing in seismic exploration, such as seismic noise attenuation (Yang et al., 2021) (Peng et al., 2025), fault identification (Wu et al., 2019) (Li et al., 2024b), microseismic pick-up (Zhang et al., 2020), seismic face recognition (Zhang et al., 2021), seismic wavefield evolution (Zhu et al., 2025b), and seismic inversion (Wu et al., 2021) (Liu et al., 2025). Das et al. (2019) first introduced convolutional neural network (CNN) to AII, laying the foundation for the subsequent development of DL in AII. DL methods can effectively solve ill-posed nonlinear inversion problems and do not require a priori knowledge of physical models. Recently, researches on AII primarily focus on DL, with notable structural innovations that can be broadly divided into two stages, as illustrated in Figure 1(a-b). The early DL models used for AII are based on supervised learning strategies (Das et al., 2019) (Mustafa et al., 2019) (Ning et al., 2024). They establish a nonlinear relationship between seismic traces and acoustic impedance through labels (acoustic impedance well-logging data), and directly transferred this relationship to unlabeled seismic traces for AII (Zhu et al., 2025a). Wu et al. (2022) proposed the use of residual network (Resnet) to complete the supervised AII task; Zhu et al. (2022) proposed a multi-scale supervised AII to ensure the energy consistency of seismic signals in different frequency bands; Li et al. (2024a) introduced the self-attention mechanism into AII. However, supervised learning struggles to achieve bet-

a) Supervised Learning



b) Semi-Supervised Learning



c) Proposed method

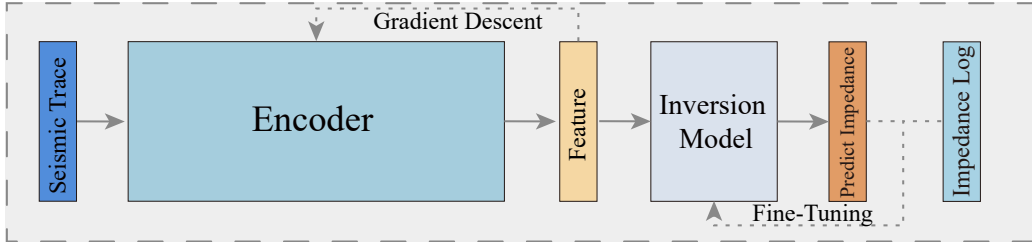


Figure 1: a) supervised learning; b) semi-supervised learning; c) proposed method based on feature exaction and fine-tuning.

ter performance, primarily due to the scarcity of well-logging data, which is limited by well logging costs.

AII can be regarded as a few-shot (Song et al., 2023) DL problem because there is less impedance well-logging data available for supervised learning (traces with well-logging data typically account for approximately 1% to 5% of the total seismic traces). To alleviate this issue, many researchers have proposed semi-supervised learning methods (Luo et al., 2023) (Lang et al., 2024) (Yuan et al., 2022), as shown in Figure 1(b). The idea of semi-supervised learning is to add a forward model to the original supervised model. For the inversion results of unlabeled traces, the forward model can be used to constrain the inversion model (Zhang et al., 2025). The semi-supervised DL method can be divided into two types: one is a physics-driven forward model (Alfarraj and AlRegib, 2019), and the other is a data-driven forward model (Liu et al., 2024). Methods using physics-driven forward models face difficulties similar to traditional approaches, namely the need to extract seismic wavelets during forward model calculations. Physics-driven forward models typically require seismic wavelets, followed by forward synthesis of seismic data (Su et al., 2023). To avoid the impacts caused by wavelet extraction, many authors have proposed using data-driven DL models as a substitute (Sang et al., 2023) (Shi et al., 2024) (Yuan et al., 2022). At this point, DL methods for AII have established a relatively mature framework, under which many authors have made improvements to DL models. Feng et al. (2025) proposed an attention mechanism-based dual-branch inversion model, which can extract multi-scale sequential features; Sun et al. (2024) proposed a fusion neural network that can invert porosity and acoustic impedance simultaneously to improve inversion performance; Pang et al. (2025) proposed a semi-supervised DL algorithm with iterative gradient correction, which enhances the robustness of the inversion model. Additionally, it is worth noting that most DL methods still employ initial models to enhance the effectiveness of inversion (Pang et al., 2025) (Gao et al., 2024).

Due to the extremely small proportion of labeled traces (seismic traces containing well-logging data), AII always faces the challenges of extrapolation or interpolation, and how to enhance the extrapolation and interpolation performance of the DL model has become a critical issue in AII. To alleviate this problem, in this work, we propose a new DL framework based on feature extraction and fine-tuning, as shown in Figure 1(c). The processing idea of the proposed method is to train a well-performing encoder that can effectively map seismic trace to linear features in high-dimension. By linearizing the

relationship between labeled and unlabeled seismic traces, the complexity of the model in processing unlabeled traces is reduced, and similar ideas have been effectively validated in some works (Webb et al., 2020) (Na and Park, 2022). To achieve this goal, we propose an extremely lightweight (less than 1k learnable parameters) model Dimension Reducer to assist in encoder training. Meanwhile, we propose Reconstructor to prevent the encoder from diverging, which reconstructs the extracted features back into seismic data. Finally, the well-trained encoder and a small amount of impedance well-logging data are used for fine-tuning the inversion model. To avoid shortcut learning during the training of the encoder (Geirhos et al., 2020), both the Reconstructor and the inversion model adopt structures different from that of the encoder. Since the proposed method does not involve a forward model, it does not require extracting seismic wavelets or training a forward model, and it can achieve good results without initial model. We conducted experiments on multiple datasets while keeping hyperparameters unchanged, and the results show that the proposed method can achieve better robustness and performance compared with supervised and semi-supervised methods. Moreover, we open-sourced the source code and data, with the hope of making contributions to the DL work in the AII field.

2. Methods

2.1. Forward modeling

Seismic acoustic impedance can generally effectively reflect the characteristics of underground reservoir and is a commonly used parameter in oil and gas mineral exploration, which is defined as

$$I = V_p \times D, \quad (1)$$

where V_p represents the P-wave velocity and D represents the density. I can only be measured by well logging and it is very costly, which means that I data is scarce.

Seismic records can reflect the distribution of acoustic impedance to a certain extent. Typically, seismic record can be regarded as being obtained by convolving the reflection coefficient with the seismic wavelet (Robinson, 1967):

$$S(t) = R(t) * W(t) + n(t), \quad (2)$$

where t represents sampling time, S represents the seismic record, and R represents the reflection coefficient sequence. n represents a small amount of random noise, which can generally be eliminated using noise attenuation techniques. Additionally, the reflection coefficient sequence can be constructed using acoustic impedance:

$$R(t) = \frac{I_{t+\Delta t} - I_t}{I_{t+\Delta t} + I_t}. \quad (3)$$

Combining Equation 2 and 3 can achieve the synthesis from acoustic impedance to seismic records. However, although forward modeling is relatively simple, the inverse solution for acoustic impedance is very difficult.

2.2. Encoder-Inverter framework

Due to the fact that the AII problem cannot be directly addressed, traditional optimization methods have limitations (such as requiring an accurate initial model and seismic wavelets), and many authors have resorted to using DL methods for processing. Most works focus on how to improve the generalization of models while neglecting the processing of the data itself. It is assumed that there are x consecutive seismic traces $\{S_1(t), S_2(t), \dots, S_x(t)\}$, and their original features are characterized by a non-linear function $S_x(t) = f(x, t)$, which is difficult to obtain. The non-linearity of f makes it difficult to measure the relationship between S_x , thus making the interpolation or extrapolation of AII complex. To alleviate this issue, we propose two improvements: first, decompose f into a high-dimensional linear function through an encoder; second, use a linear layer-based model to construct the Inverter, as multilayer perceptron exhibit strong linear extrapolation capabilities (Xu et al., 2021).

Generally speaking, linear tasks are usually easier to solve than non-linear tasks (Elizondo et al., 2012). For the Inverter, when the input seismic trace features are linear and supervised learning can be carried out using few labeled traces, the AII problem for unlabeled traces is transformed into linear extrapolation or interpolation of the Inverter, thereby reducing the complexity of AII. To achieve this goal, we propose two auxiliary models, Dimension Reducer and Reconstructor, for training Encoder, which will be described in the following sections. Finally, after the encoder is trained, a small amount of well-logging data is used to fine-tune the Inverter. During the entire process, well-logging data is only used for fine-tuning the Inverter. Additionally, the

proposed Inverter has a very simple structure, capable of achieving excellent inversion results without requiring additional forward models or initial models.

2.3. Structure of models

The structure of the proposed model and the training strategy are shown in Figure 2. The Encoder has a relatively complex structure, consisting of four temporal convolutional network (TCN) blocks; the Inverter and Reconstructor share the same structure, which is constructed via bidirectional gated recurrent units (Bi-GRU) and linear layers; the Dimension Reducer is designed to implement an adaptive dimensionality reduction strategy for features, so it is built with only one layer of Bi-GRU and a linear layer, with a total number of learnable parameters of less than 1k (which varies according to the length of seismic traces). The entire proposed model maintains a lightweight design, with a total of approximately 108k learnable parameters.

2.3.1. Encoder

In AII tasks, the TCN has been proven to be a highly effective structure and is widely used in many studies (Shi et al., 2024) (Feng et al., 2025). TCN is time series processing model based on CNN. Through structures such as dilated convolution and residual connection, it can effectively capture temporal dependency relationships in long sequences. Mustafa and AlRegib (2021) deeply discussed the impact of different TCNs on inversion performance, which shows that non-causal TCN exhibit the best performance in AII. The structures of causal TCN and non-causal TCN are shown in Figure 3, taking dilation of 2 as an example.

Since the forward synthetic of seismic records demonstrated in Equation 2 and 3 is not a causal process (Mustafa and AlRegib, 2021), the model for AII should inherently be non-causal, which has been validated in practice (Liu et al., 2025). Increasing dilation allows TCN to handle long-sequence information, but it requires more channels (more kernels) to preserve sequence details; conversely, reducing or eliminating dilation necessitates deeper networks to expand the receptive field. Furthermore, we aim to map seismic traces into a high-dimensional space for linear representation. Therefore, in this work, we constructed an over-complete encoder using four TCN blocks and its structure is shown in Figure 2(c). Each TCN block is composed of two layers of TCN, two Tanh activation functions, and residual connection.

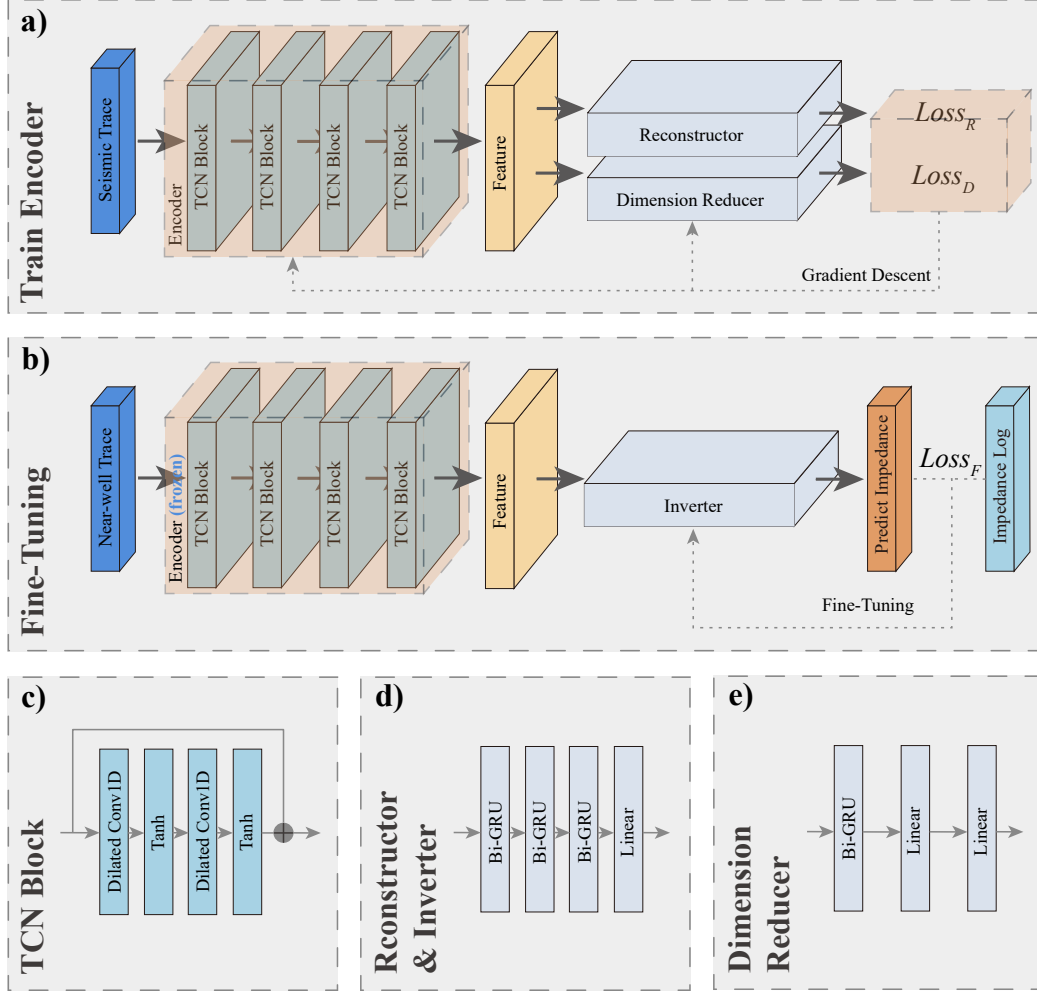


Figure 2: a) the structure of Encoder and its training strategy; b) the fine-tuning of Inverter; c), d), and e) respectively represent the structures of TCN block, Inverter, Reconstructor, and Dimension Reducer.

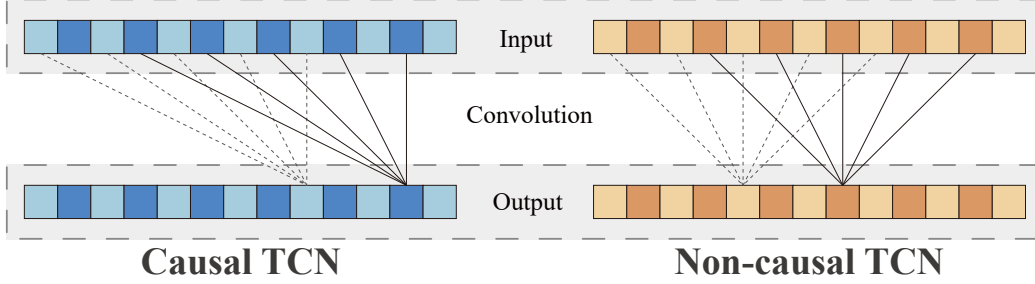


Figure 3: The structure of causal and non-causal TCN, with dilation of 2.

2.3.2. Dimension Reducer

As mentioned above, we hope that the features after passing through the Encoder can be as linearly separable as possible, transforming the transfer learning of the inversion model (from labeled seismic traces to unlabeled seismic traces) into linear extrapolation or interpolation. Therefore, the high-dimensional features encoded by the Encoder should be representable by high-dimensional straight lines:

$$F_m^x = A_{m \times 1} \times x + B_{m \times 1}, \quad (4)$$

where $F_m^x \in \{F_m^1, F_m^2, \dots\}$ represents features of seismic trace S_x and $A_{m \times 1} \times x + B_{m \times 1}$ is a straight line in an m -dimensional space. However, this line is difficult to calculate directly, so we propose Dimension Reducer for constraint. First, transform the above equation to obtain

$$x = \frac{A_{m \times 1}^\top}{A_{m \times 1}^\top A_{m \times 1}} (F_m^x - B_{m \times 1}), \quad (5)$$

the Equation 5 is in the form of a standard linear layer. The architecture of Dimension Reducer we constructed is shown in Figure 2(e). In addition to two linear layers (respectively used for reduction of channels and sequence length), we added a Bi-GRU layer which is a time-series processing model constructed using linear layers, designed to better constrain temporal features. Since Dimension Reducer is a simple and lightweight network, containing only approximately 1k parameters, it can form a good constraint on the Encoder through gradient descent and this strategy has been widely used for feature alignment in some domain adaptation works (Ganin et al., 2016).

2.3.3. *Reconstructor and Inverter*

In our experiments, we found that constraining the Encoder with only the dimension reducer made it difficult for the entire model to converge because this single condition alone cannot guarantee the effectiveness of the extracted features. Therefore, we propose Reconstructor to further constrain the encoder, which is shown in Figure 2(d). The Reconstructor ensures that the extracted features can be reconstructed back into seismic traces, and its structure is composed of three layers of Bi-GRU and linear layer. For the Inverter, we adopt the same structure as Reconstructor.

On the one hand, Bi-GRU is constructed through linear layers and non-linear activation functions. Linear layers exhibit strong linear extrapolation capabilities (Xu et al., 2021), while non-linear activation functions effectively ensure that non-linear features in acoustic impedance can be learned. On the other hand, adopting different architectures helps the model extract more robust features. During the training of the Encoder, if the Reconstructor shares an identical or similar structure with the Encoder, the extracted features will bias toward the reconstruction task (as Geirhos et al. (2020) discussed, models often find shortcut solutions, making the model difficult to transfer), which degrades the performance of AII.

Moreover, Bi-GRU possesses excellent long-sequence modeling capabilities and is one of the most commonly used structures in the AII field. It can complete sequence modeling without requiring a very deep structure, avoiding overfitting of the Reconstructor and the Inverter.

2.4. *Inversion workflow*

Based on the previous sections, the AII processing workflow proposed in this work can be divided into two parts: training of the Encoder and fine-tuning of the Inverter. First, we train the Encoder using all seismic trace records with the Reconstructor and Dimension Reducer, as shown in Figure 2(a) and Algorithm 1. During the training of Dimension Reducer and Reconstructor via gradient descent, effective constraints are imposed on the encoder (Ganin et al., 2016).

Second, the trained Encoder and a small number of labeled seismic traces are used to train the Inverter, which is the fine-tuning stage and is shown in Figure 2(b) and Algorithm 2. In AII tasks, well-logging data is typically scarce, and the seismic traces with well-logging data as the true acoustic impedance account for only 1% to 5% of the total seismic traces. By applying

Algorithm 1 Training of the Encoder

Input: Seismic traces $\{S_1, S_2, \dots, S_x\}$; Initialized Encoder $E(\theta_E)$, Reconstructor $R(\theta_R)$, and Dimension Reducer $D(\theta_D)$

Output: Well-trained parameters θ_E

```
1  for  $i = 1$  to  $Max\ Epoch$  do
2    for  $j = 1$  to  $Max\ Batch$  do
3      Randomly extract  $S_x$  from the seismic traces set
4      Encode the seismic trace:  $F_m^x \leftarrow E(S_x, \theta_E)$ 
5      Reduce the dimension of  $F_m^x$ :  $x' \leftarrow D(F_m^x, \theta_D)$ 
6      Reconstruct the seismic trace:  $S'_x \leftarrow R(F_m^x, \theta_R)$ 
7      Calculate the  $Loss_D$ :  $Loss_D \leftarrow \|x - x'\|_2^2$ 
8      Calculate the  $Loss_R$ :  $Loss_R \leftarrow \|S_x - S'_x\|_2^2$ 
9      Optimize the model parameters:  $\arg \min_{\theta_E, \theta_D, \theta_R} (Loss_R + Loss_D)$ 
10 Return: trained parameters  $\theta_E$ 
```

the trained Inverter and Encoder to all seismic traces, the AII work can be completed.

Algorithm 2 Fine-tuning of the Inverter and AII

Input: Seismic traces $\{S_1, S_2, \dots, S_x\}$; Few seismic traces $\{S_1, S_2, \dots, S_z\}$ and matching well-logging data $\{I_1, I_2, \dots, I_z\}$, where $z \ll x$; Well-trained Encoder parameters θ_E ; Initialized Inverter $Inv(\theta_{Inv})$

Output: Acoustic Impedance $\{I_1, I_2, \dots, I_x\}$

```
// fine-tuning of the Inverter
1  for  $i = 1$  to  $Max\ Epoch$  do
2    for  $j = 1$  to  $Max\ Batch$  do
3      Randomly extract matching  $S_z$  and  $I_z$  from the seismic traces and well-logging data set
4      Encode the seismic trace:  $F_m^z \leftarrow E(S_z, \theta_E)$ 
5      Inversion:  $I'_z \leftarrow Inv(F_m^z, \theta_{Inv})$ 
6      Calculate the loss function  $Loss_F$ :  $\|I_z - I'_z\|_2^2$ 
7      Optimize the model parameters:  $\arg \min_{\theta_{Inv}} Loss_F$ 

// AII process
8  for  $i = 1$  to  $x$  do
9     $I_i \leftarrow Inv(E(S_i, \theta_E), \theta_{Inv})$ 
10 Return: inverted acoustic impedance  $\{I_1, I_2, \dots, I_x\}$ 
```

In the next section, three most widely used open-source datasets are used for comparative experiments to verify the effectiveness and computational efficiency of the proposed Encoder-Inverter framework.

3. Experiment

3.1. Datasets and evaluation metrics

In this experiment, we use three datasets and conducted experimental validations on each dataset individually, ensuring no cross-utilization of data

across different datasets. The three datasets are: Overthrust (Aminzadeh et al., 1996), SEAM elastic earth model (Capello et al., 2017), and Marmousi 2 (Martin et al., 2006). During the past decade, these three datasets have been adopted in nearly all AII tasks for validation, and the relevant parameters of these three datasets are shown in Table 1. As can be seen, in each dataset, we use fewer than 1% of the seismic traces as labeled traces, which is far lower than the proportion used in many AII studies. Since the Marmousi 2 dataset contains more complex structures and is more challenging to process, we use more well-logging data, but it is still less than that used in other works.

Dataset	Trace Num	Well Num	Time Interval	Record Time
Overthrust	1067	10 (<1%)	4ms	3s
Marmousi 2	1701	14 (<1%)	3ms	2.4s
SEAM	1751	10 (<1%)	4ms	5s

Table 1: The parameters of Overthrust, Marmousi 2 and SEAM datasets

During the training of the Encoder, we use the Adam optimizer for gradient descent with a learning rate of 0.001. Due to the large number of seismic traces and the relatively simple encoder structure, convergence is achieved in approximately 30 epochs. In the fine-tuning stage, due to the greater optimization difficulty of AII, we use a larger learning rate (0.01) and more epochs (1,000) for training the Inverter.

In addition, five metrics are adopted in this work to conduct accurate comparative experiments. The first metric is the signal-to-noise ratio (SNR), which is commonly used in the field of signal processing and can be expressed as

$$SNR = 10 * \log_{10} \frac{\sum_{i=1}^N I_i^2}{\sum_{i=1}^N (I_i - I'_i)^2} \quad (6)$$

where I represents the true wave impedance and I' represents the predicted acoustic impedance. The SNR describes the logarithmic ratio between the true impedance and the prediction error, and a larger value is better. The second metric is R^2 , the most commonly used evaluation metric in AII, which

is defined as

$$R^2 = 1 - \frac{\sum_{i=1}^N (I_i - I'_i)^2}{\sum_{i=1}^N (\mu_I - I_i)^2}, \quad (7)$$

where μ_I is the mean of I . Structural similarity (SSIM) is a commonly used metric in the field of image processing, used to describe the similarity between two images, and it is also used in many works of AII. Its definition is

$$SSIM = \frac{(2 \times \mu_I \times \mu_{I'} + c_1)(2 \times \sigma_{II'} + c_2)}{(\mu_I^2 + \mu_{I'}^2 + c_1)(\sigma_I^2 + \sigma_{I'}^2 + c_2)}, \quad (8)$$

where σ_I^2 represents the variance of I , $\sigma_{I'}^2$ represents the variance of I' , and $\sigma_{II'}$ represents the covariance between I and I' . c_1 and c_2 are very small positive values to avoid a zero denominator. SSIM generally pays more attention to global deviations and is less affected by local errors. Mean absolute error (MAE) and mean squared error (MSE) are two commonly used metrics in regression tasks, and their calculation methods can be expressed as

$$MAE = \frac{1}{N} \sum_{i=1}^N |I_i - I'_i|, \quad (9)$$

$$MSE = \frac{1}{N} \sum_{i=1}^N (I_i - I'_i)^2. \quad (10)$$

These two metrics fluctuate with the numerical range of the data, so we standardize (Z-Score) I and I' before calculating them.

In the next section, we will use the above metrics to conduct comparative evaluations with the datasets. Additionally, to ensure the reproducibility of our experimental results, we will open-source these datasets along with the reproducible code.

3.2. Overthrust

The Overthrust is a relatively simple dataset, created by the SEG/EAGE 3-D Modeling committee (Aminzadeh et al., 1996). In this task, we adopted four open-source methods for comparison, which are supervised CNN (Das et al., 2019), supervised TCN (Mustafa et al., 2019), semi-supervised model with physics-forward (semi-supervised PF) (Alfarraj and AlRegib, 2019), and semi-supervised model with model-forward (semi-supervised MF) (Shi et al., 2024). In addition, we also add a comparative experiment on the Dimension

Reducer to determine its effectiveness. Figures 4(a) and (b) show the seismic data of Overthrust and the true impedance, respectively. We extracted 10 seismic traces at equal intervals as label traces, as shown in Figure 4(b), for AII processing.

It can be seen that the most challenging part of AII lies in the sharply changing partial data, which have larger deviations due to the lack of well-logging data. As shown in Figures 4(e) and (f), the processing results of the two supervised methods are slightly inferior to those of the other three methods, with more identification errors. In Figure 4(c), the results of the proposed Encoder-Inverter framework have a higher resolution, can clearly and accurately identify structures such as faults. When there is no Dimension Reducer (Figure 4(d)), the lateral continuity is slightly reduced, which becomes more evident in more complex data. Although the two semi-supervised methods outperform the two supervised methods, they also face the problem of insufficient resolution and exhibit more obvious vertical artifacts (Figures 4(g) and (h)). This is more intuitively demonstrated in the absolute residuals, as shown in Figure 5.

From Figures 5(c) and (d), it can be clearly seen that the supervised methods have larger deviations, which are unfavorable for quantitative interpretation. Followed by the two semi-supervised methods in Figures 5(e) and (f), the semi-supervised PF is affected by the extracted wavelets, which reduces the overall performance of the semi-supervised methods. In contrast, adopting a model-driven forward model can effectively address this issue. In the absence of Dimension Reducer, the proposed method can achieve results comparable to semi-supervised MF, which is shown in Figure 5(b). Additionally, incorporating Dimension Reducer effectively enhances the performance of the proposed method, indicating that linear encoding of seismic traces can significantly improve the Inverter’s ability to process non-label traces. To more intuitively demonstrate the deviations of different methods, we plot scatterplots of the predicted impedance versus the true impedance, as shown in Figure 6. As can be seen in Figure 6(a), the results of the proposed method have smaller deviations compared to other methods. The supervised MF, the supervised PF, and the proposed method without Dimension Reducer follows (Figures 6(b), (e), and (f)), with only a few regions showing larger deviations than the proposed method. Finally, we select three inverted traces for display, as shown in Figure 7, it can also be intuitively seen the effectiveness of the proposed method. Overall, the structure of the Overthrust dataset is relatively simpler. Therefore, in the next section, we will use a more complex

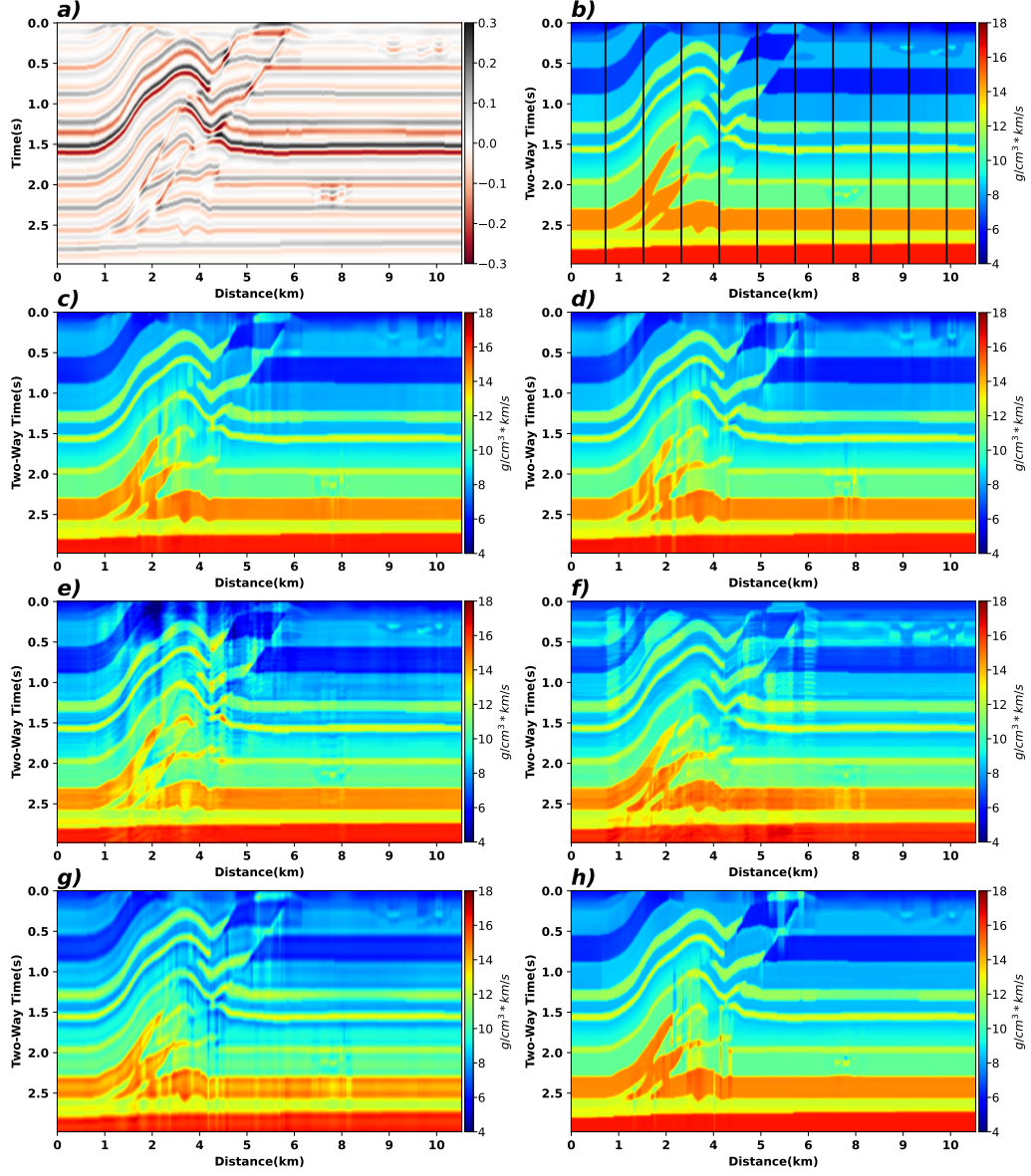


Figure 4: The seismic data, true acoustic impedance and AII results of Overthrust. a) seismic data; b) ground truth and wells; c) results of proposed method; d) results of proposed method without Dimension Reducer; e) results of supervised CNN; f) results of supervised TCN; g) results of semi-supervised PF; h) results of semi-supervised MF.

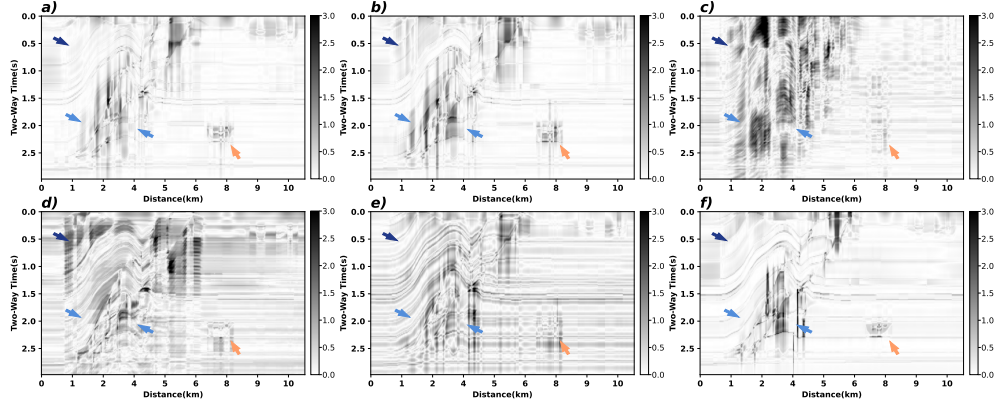


Figure 5: The absolute residuals of results. a) absolute residuals of proposed method; b) absolute residuals of proposed method without Dimension Reducer; c) absolute residuals of supervised CNN; d) absolute residuals of supervised TCN; e) absolute residuals of semi-supervised PF; f) absolute residuals of semi-supervised MF.

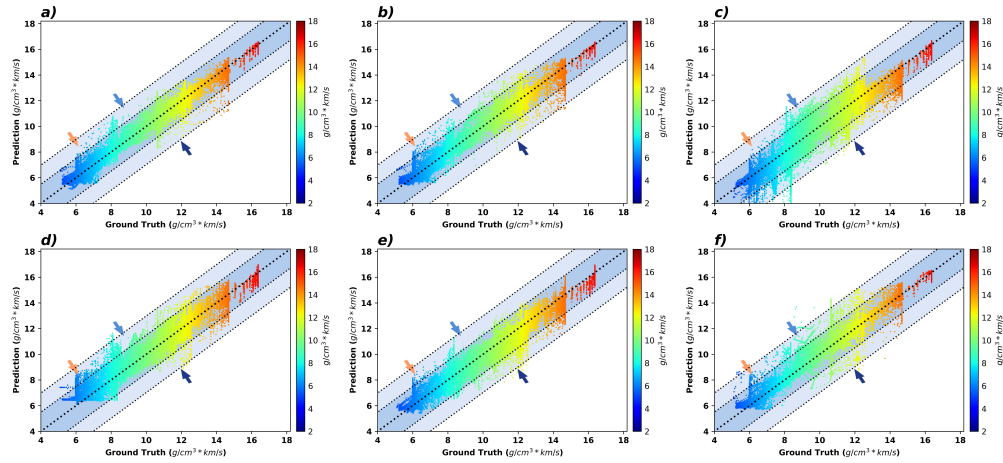


Figure 6: The scatterplots of results and true acoustic impedance. a) scatterplot of proposed method; b) scatterplot of proposed method without Dimension Reducer; c) scatterplot of supervised CNN; d) scatterplot of supervised TCN; e) scatterplot of semi-supervised PF; f) scatterplot of semi-supervised MF.

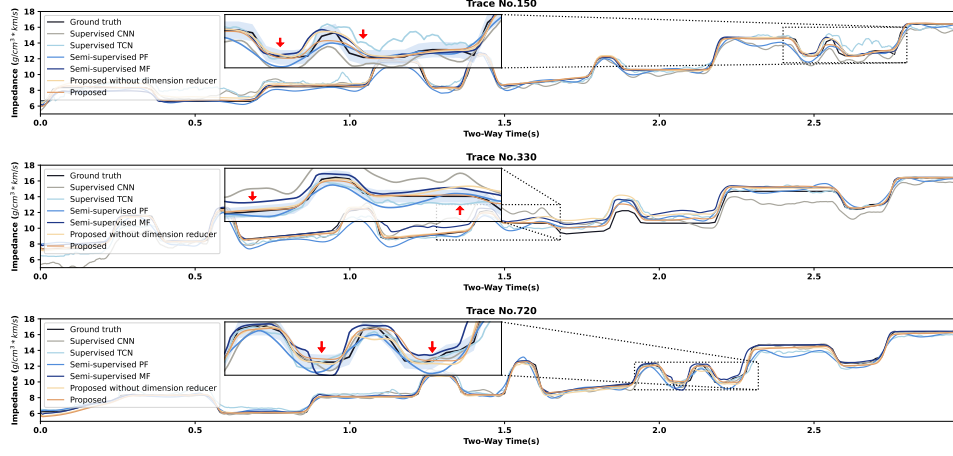


Figure 7: Acoustic inversions of trace No.150, No.330, and No.720

dataset for comparative experiments.

3.3. *Marmousi 2*

The AGL elastic Marmousi dataset, commonly known as the Marmousi 2 dataset, is created by [Martin et al. \(2006\)](#). This is a complex dataset, with a lateral extension of 17 kilometers and a depth of 3.5 kilometers, and it is the most widely used dataset in the AII field. In this dataset, we use 14 traces as labeled traces, which is far fewer than the number of traces used in other works, and the seismic data and the labeled traces used are shown in Figure 8(a) and (b).

Although Marmousi 2 is more complex than Overthrust, the proposed method still achieves better results (Figure 8(c) and Figure 9(a)) and shows a more significant gap compared to other methods. In contrast, the two supervised methods, especially the supervised CNN, exhibit more obvious overall deviations and artifacts (Figure 8(e) and Figure 9(c)); Although the supervised TCN can invert the overall trend of acoustic impedance, it struggles to achieve good results in weak reflection areas and regions with high detail (Figure 8(f) and Figure 9(d)). The processing results of the two semi-supervised methods differ significantly. Semi-supervised PF exhibits more obvious overall deviations, particularly in weak reflection areas (Figure 8(g) and Figure 9(e)). In contrast, semi-supervised MF performs better in weak reflection regions but shows poorer results in areas with sharp changes (Figure 8(h) and Figure 9(f)). These deviations can be more intuitively observed

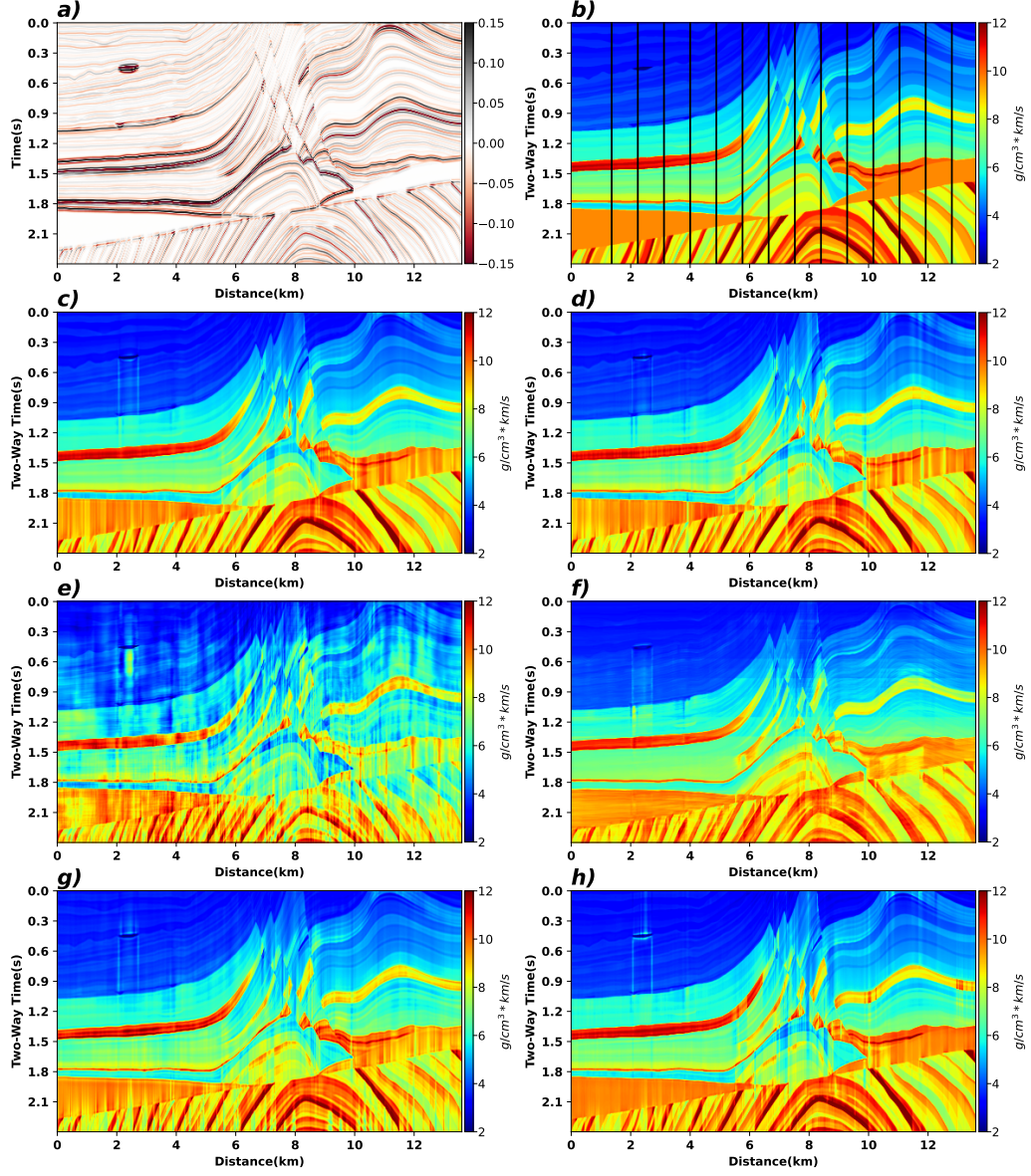


Figure 8: The seismic data, true acoustic impedance and AII results of Marmousi 2. a) seismic data; b) ground truth and wells; c) results of proposed method; d) results of proposed method without Dimension Reducer; e) results of supervised CNN; f) results of supervised TCN; g) results of semi-supervised PF; h) results of semi-supervised MF.

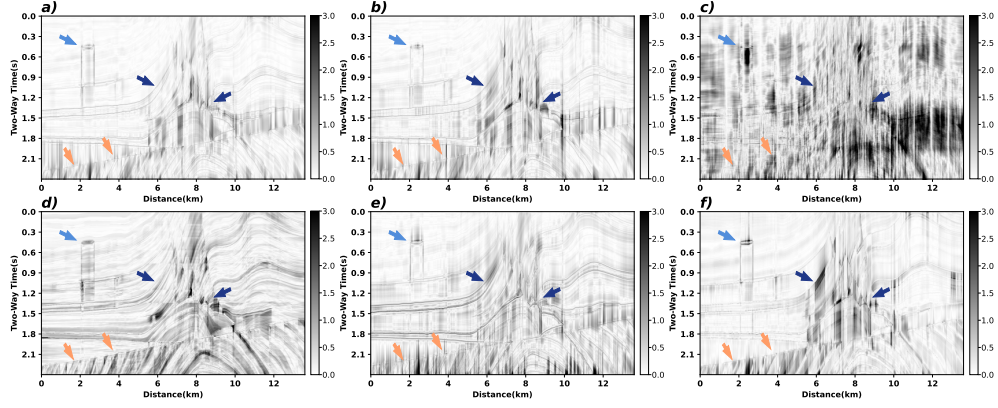


Figure 9: The absolute residuals of results. a) absolute residuals of proposed method; b) absolute residuals of proposed method without Dimension Reducer; c) absolute residuals of supervised CNN; d) absolute residuals of supervised TCN; e) absolute residuals of semi-supervised PF; f) absolute residuals of semi-supervised MF.

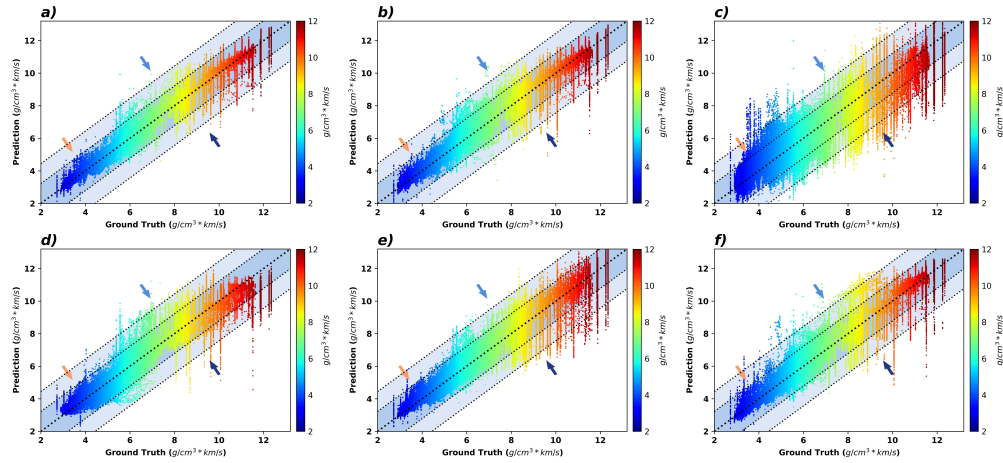


Figure 10: The scatterplots of results and true acoustic impedance. a) scatterplot of proposed method; b) scatterplot of proposed method without Dimension Reducer; c) scatterplot of supervised CNN; d) scatterplot of supervised TCN; e) scatterplot of semi-supervised PF; f) scatterplot of semi-supervised MF.

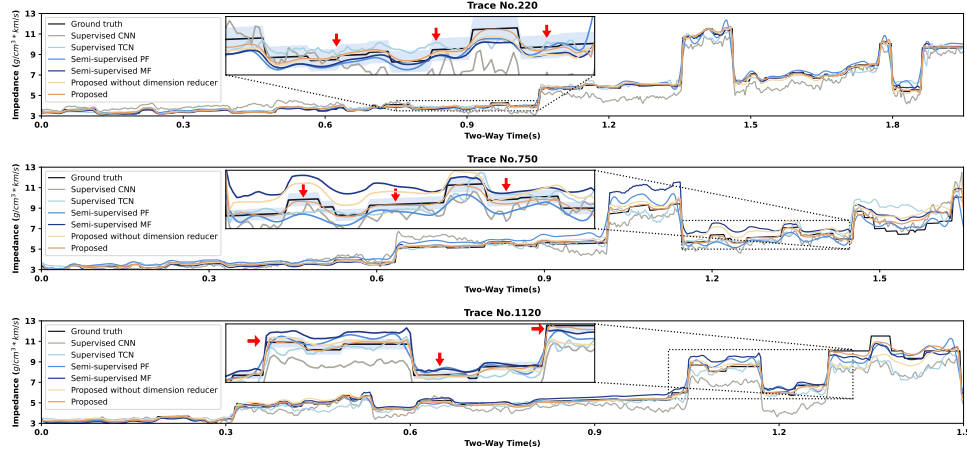


Figure 11: Acoustic inversions of trace No.220, No.750, and No.1120.

through the scatterplots, as shown in Figure 10.

As clearly shown in Figures 10(a) and (b), the proposed Dimension Reducer effectively constrains the encoder to meet our expectations. Under the linear constraint of features, the overall error of AII is significantly reduced. Similarly, we display several inverted seismic traces, with the results shown in Figure 11. It can be seen that the structure of the Marmousi 2 model is relatively complex, and meanwhile, the result differences among various methods are more obvious.

3.4. SEAM

The SEAM elastic earth model includes a 35km survey line, and all its properties are derived from basic rock properties (Capello et al., 2017). In addition to containing a sandstone body, SEAM has a very rich number of thin layers (Figure 12(a)), which is conducive to evaluating the accuracy of AII methods.

It can be clearly seen that constrained by single supervised learning, the supervised CNN almost fails (Figure 12(e)), and details are almost lost in the results of the supervised TCN (Figure 12(f)). These deviations are more intuitively demonstrated in Figures 13(c) and (d), where the supervised CNN fails in the AII of sandstone body and the supervised TCN loses almost all thin layers. Semi-supervised PF shows improvements in thin layer regions compared to the two supervised learning methods (Figure 12(g) and Figure 13(e)); however, it still has significant errors in sandstone body regions.

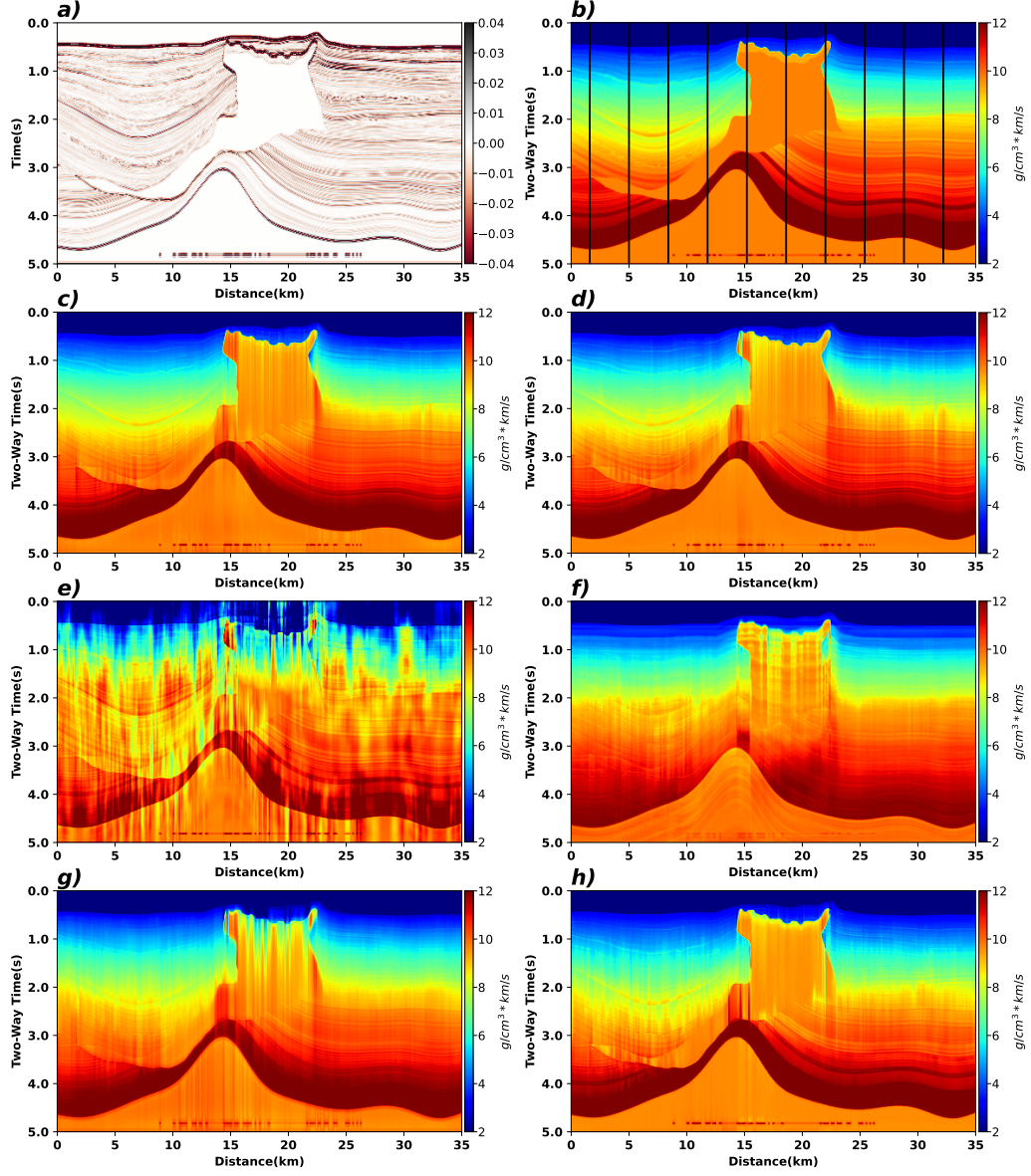


Figure 12: The seismic data, true acoustic impedance and AII results of SEAM. a) seismic data; b) ground truth and wells; c) results of proposed method; d) results of proposed method without Dimension Reducer; e) results of supervised CNN; f) results of supervised TCN; g) results of semi-supervised PF; h) results of semi-supervised MF.

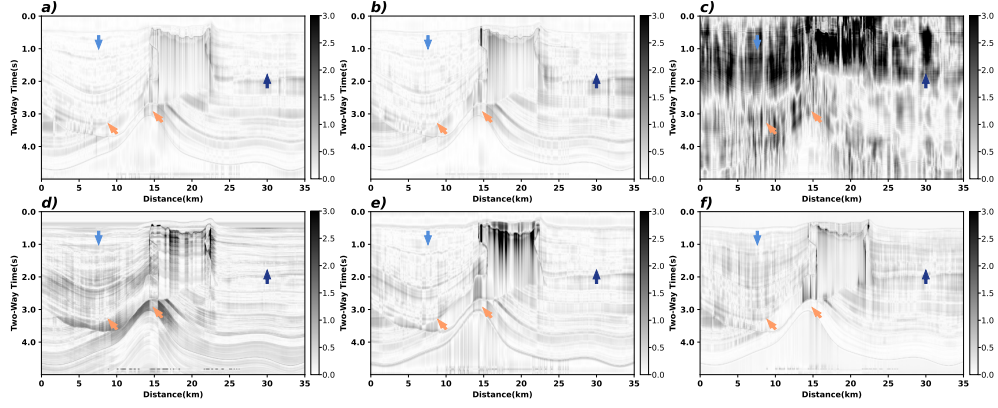


Figure 13: The absolute residuals of results. a) absolute residuals of proposed method; b) absolute residuals of proposed method without Dimension Reducer; c) absolute residuals of supervised CNN; d) absolute residuals of supervised TCN; e) absolute residuals of semi-supervised PF; f) absolute residuals of semi-supervised MF.

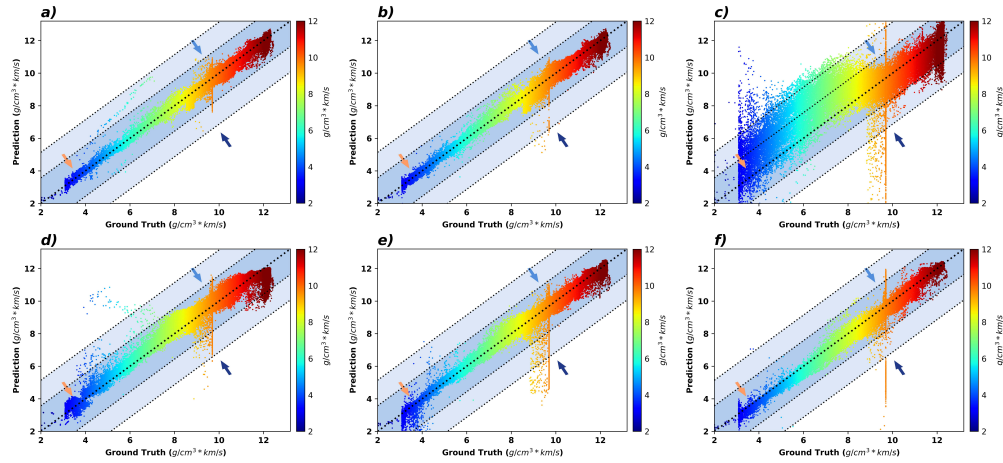


Figure 14: The scatterplots of results and true acoustic impedance. a) scatterplot of proposed method; b) scatterplot of proposed method without Dimension Reducer; c) scatterplot of supervised CNN; d) scatterplot of supervised TCN; e) scatterplot of semi-supervised PF; f) scatterplot of semi-supervised MF.

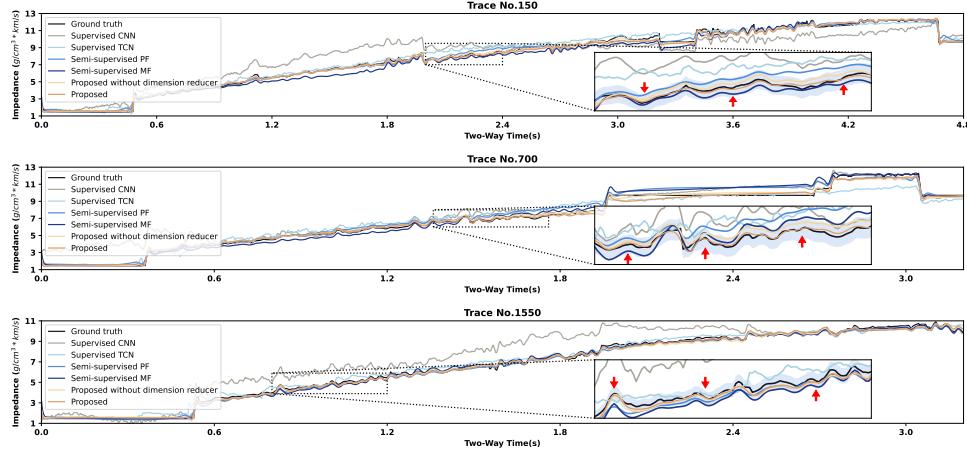


Figure 15: Acoustic inversions of trace No.150, No.700, and No.1550.

In contrast, semi-supervised MF demonstrates a notable improvement over semi-supervised PF (Figure 13(f)). Besides, the proposed method achieves the best results, with overall errors being smaller than other methods in both thin layer and sandstone body regions (Figure 13(a) and Figure 14(a)). In Figure 14, it can be seen that except for minor deviations in very few regions, the proposed method generally maintains relatively small deviations, which outperforms other comparative methods.

Finally, in Figure 15, we extract three inverted seismic traces for demonstration. It can be clearly seen that compared with the above two datasets, the SEAM dataset contains more thin layers or weak reflection regions, which poses a challenge to AII work. In this case, the two supervised methods almost failed, and the proposed method significantly has smaller errors and is closer to the true acoustic impedance compared with the two semi-supervised methods.

3.5. Quantitative results

In this section, we use five metrics to quantify the deviations of the results from various methods, as shown in Table 2. Our proposed method achieves the best results across five metrics on three datasets. Additionally, when without Dimensional Reducer, the proposed method can achieve performance comparable to semi-supervised MF. This result indicates that the linear feature constraints proposed in this task have played a significant role. The linear features effectively improve the performance of the Inverter in

processing non-labeled traces, ultimately leading to better AII results. It is worth noting that supervised methods can be effective when dealing with relatively simple datasets, but their performance is difficult to guarantee when processing complex datasets with a lack of well-logging data.

Metric	Dataset	Proposed	Proposed (without Dimension Reducer)	Supervised CNN	Supervised TCN	Semi-supervised PF	Semi-supervised MF
SNR \uparrow	Overthrust	30.8307	29.5747	25.2185	25.3310	27.0136	29.1915
	Marmousi 2	25.7436	23.9952	16.6838	21.7474	22.3415	23.3248
	SEAM	31.5077	30.3421	16.2672	25.0340	25.3898	28.6047
R^2 \uparrow	Overthrust	0.9892	0.9856	0.9606	0.9616	0.9740	0.9842
	Marmousi 2	0.9783	0.9675	0.8250	0.9455	0.9524	0.9621
	SEAM	0.9944	0.9926	0.8112	0.9749	0.9769	0.9890
SSIM \uparrow	Overthrust	0.9542	0.9330	0.8733	0.8587	0.8809	0.9359
	Marmousi 2	0.9134	0.8907	0.7556	0.8108	0.8355	0.8827
	SEAM	0.9277	0.9131	0.7598	0.8296	0.8711	0.9245
MAE \downarrow	Overthrust	0.0579	0.0674	0.1163	0.1346	0.1126	0.0627
	Marmousi 2	0.0914	0.1128	0.3116	0.1602	0.1444	0.1130
	SEAM	0.0497	0.0547	0.3006	0.1086	0.0851	0.0583
MSE \downarrow	Overthrust	0.0108	0.0145	0.0386	0.0351	0.0244	0.0153
	Marmousi 2	0.0217	0.0327	0.1721	0.0547	0.0480	0.0369
	SEAM	0.0055	0.0072	0.1941	0.0243	0.0227	0.0088

Table 2: The quantitative metrics of various methods on Overthrust, Marmousi 2 and SEAM datasets.

There are also significant differences between the two semi-supervised methods. First, the semi-supervised method using a physics-driven forward process relies on the extraction of seismic wavelets, and its processing results are largely constrained by the accuracy of the wavelets. Second, the semi-supervised method using a DL model-driven forward process can effectively alleviate this issue. However, the effectiveness of such data-driven constraints is difficult to guarantee, and there is still room for improvement in this framework. Different from previous methods, the Encoder-Inverter framework is a new structure which features strong robustness and AII performance, and has achieved significant improvements in accuracy and precision.

4. Conclusion

In this work, we propose Encoder-Inverter framework, a brand-new framework for seismic acoustic impedance inversion. We design two additional

models for the training of the Encoder, decomposing seismic traces into a linear feature space, and using the decomposed linear features and a small amount of well-logging data to fine-tune the Inverter. The role of linear features lies in transforming the acoustic impedance inversion of non-labeled seismic traces into an extrapolation or interpolation task of Inverter, thereby improving the inversion performance. To achieve this objective, we introduce two auxiliary models, the Dimension Reducer and the Reconstructor: the Dimension Reducer is designed to ensure the extraction of linear features from seismic trace; and the Reconstructor serves to validate the effectiveness of the extracted features by ensuring they can be reconstructed back into seismic data, maintaining the integrity and usability of the features for subsequent inversion tasks. We conducted comparative experiments on three most commonly used datasets, comparing with supervised learning and semi-supervised learning methods, to demonstrate the effectiveness of the proposed framework. Finally, to provide a reference for future research, we will open-source the data and code of this work.

5. Acknowledgement

The code used in this work will be uploaded to github repository <https://github.com/lexiaoheng/Mariana>.

References

- Alfarraj, M., AlRegib, G., 2019. Semisupervised sequence modeling for elastic impedance inversion. *Interpretation* 7, SE237–SE249.
- Aminzadeh, F., Burkhard, N., Long, J., Kunz, T., Duclos, P., 1996. Three dimensional seg/eaeg models—an update. *The Leading Edge* 15, 131–134.
- Capello, M.A., House, N., Barkhouse, W., 2017. Seam: A 10-year trail of success grounded in sound research, collaboration, and outreach. *The Leading Edge* 36, 724–727.
- Conti, C.R., Roisenberg, M., Neto, G.S., Porsani, M.J., 2013. Fast seismic inversion methods using ant colony optimization algorithm. *IEEE Geoscience and Remote Sensing Letters* 10, 1119–1123.
- Das, V., Pollack, A., Wollner, U., Mukerji, T., 2019. Convolutional neural network for seismic impedance inversion. *Geophysics* 84, R869–R880.

- Doyen, P.M., 2007. Seismic reservoir characterization: An earth modelling perspective. EAGE.
- Elizondo, D.A., Birkenhead, R., Gamez, M., Garcia, N., Alfaro, E., 2012. Linear separability and classification complexity. *Expert Systems with Applications* 39, 7796–7807.
- Feng, W., Liu, Y., Li, Y., Li, H., Wang, X., 2025. Acoustic impedance prediction using an attention-based dual-branch double-inversion network. *Earth Science Informatics* 18, 1–20.
- de Figueiredo, L.P., Grana, D., Santos, M., Figueiredo, W., Roisenberg, M., Neto, G.S., 2017. Bayesian seismic inversion based on rock-physics prior modeling for the joint estimation of acoustic impedance, porosity and lithofacies. *Journal of Computational Physics* 336, 128–142.
- Ganin, Y., Ustinova, E., Ajakan, H., Germain, P., Larochelle, H., Laviolette, F., March, M., Lempitsky, V., 2016. Domain-adversarial training of neural networks. *Journal of machine learning research* 17, 1–35.
- Gao, Z., Guo, M., Li, C., Li, Z., Gao, J., Xu, Z., 2024. Deep learning accelerated blind seismic acoustic-impedance inversion. *IEEE Transactions on Geoscience and Remote Sensing* .
- Geirhos, R., Jacobsen, J.H., Michaelis, C., Zemel, R., Brendel, W., Bethge, M., Wichmann, F.A., 2020. Shortcut learning in deep neural networks. *Nature Machine Intelligence* 2, 665–673.
- Lang, X., Li, C., Wang, M., Li, X., 2024. Semi-supervised seismic impedance inversion with convolutional neural network and light weight transformer. *IEEE Transactions on Geoscience and Remote Sensing* .
- Li, K., Dou, Y., Xiao, Y., Jing, R., Zhu, J., Ma, C., 2024a. Transinver: 3d data-driven seismic inversion based on self-attention. *Geophysics* 89, WA127–WA141.
- Li, X., Li, K., Xu, Z., Huang, Z., 2024b. Fault-seg-lnet: A method for seismic fault identification based on lightweight and dynamic scalable network. *Engineering Applications of Artificial Intelligence* 127, 107316.

- Lin, K., Zhao, L., Wen, X., Zhang, Y., 2023. Time-frequency mixed domain multi-trace simultaneous inversion method. *Geoenergy Science and Engineering* 230, 212164.
- Lines, L., Treitel, S., 1984. A review of least-squares inversion and its application to geophysical problems. *Geophysical prospecting* 32, 159–186.
- Liu, M., Bossmann, F., Wang, W., Ma, J., 2024. Towards artifact-free impedance inversion by a semi-supervised network with super resolution and attention mechanism. *IEEE Transactions on Geoscience and Remote Sensing* .
- Liu, Y., Li, Y., Li, H., Peng, J., Liao, Z., Feng, W., Wang, M., 2025. The nash-mtl-stcn method for prestack three-parameter inversion. *Geophysics* 90, 1–74.
- Luo, R., Chen, H., Wang, B., 2023. Semisupervised seismic impedance inversion with data augmentation and uncertainty analysis. *Geophysics* 88, M213–M224.
- Mallick, S., 1995. Model-based inversion of amplitude-variations-with-offset data using a genetic algorithm. *Geophysics* 60, 939–954.
- Martin, G.S., Wiley, R., Marfurt, K.J., 2006. Marmousi2: An elastic upgrade for marmousi. *The leading edge* 25, 156–166.
- Mustafa, A., Alfarraj, M., AlRegib, G., 2019. Estimation of acoustic impedance from seismic data using temporal convolutional network, in: *SEG technical program expanded abstracts 2019*. Society of Exploration Geophysicists, pp. 2554–2558.
- Mustafa, A., AlRegib, G., 2021. A comparative study of transfer learning methodologies and causality for seismic inversion with temporal convolutional networks, in: *SEG International Exposition and Annual Meeting*, SEG. p. D011S067R001.
- Na, G.S., Park, C., 2022. Nonlinearity encoding for extrapolation of neural networks, in: *Proceedings of the 28th ACM SIGKDD Conference on Knowledge Discovery and Data Mining*, pp. 1284–1294.

- Ning, C., Wu, B., Wu, B., 2024. Transformer and convolutional hybrid neural network for seismic impedance inversion. *IEEE Journal of Selected Topics in Applied Earth Observations and Remote Sensing* 17, 4436–4449.
- Pang, Q., Chen, H., Gao, J., Wang, Z., Yang, P., 2025. Iterative gradient corrected semi-supervised seismic impedance inversion via swin transformer. *IEEE Transactions on Geoscience and Remote Sensing* .
- Peng, J., Li, Y., Liu, Y., Wang, M., Liao, Z., Wang, X., 2025. Fast diffusion model for seismic data noise attenuation. *Geophysics* 90, 1–55.
- Robinson, E.A., 1967. Predictive decomposition of time series with application to seismic exploration. *Geophysics* 32, 418–484.
- Sang, W., Yuan, S., Han, H., Liu, H., Yu, Y., 2023. Porosity prediction using semi-supervised learning with biased well log data for improving estimation accuracy and reducing prediction uncertainty. *Geophysical Journal International* 232, 940–957.
- Shaw, R., Srivastava, S., 2007. Particle swarm optimization: A new tool to invert geophysical data. *Geophysics* 72, F75–F83.
- Shi, S., Li, M., Wang, J., Chang, W., Li, L., Xie, D., 2024. Seismic impedance inversion based on semi-supervised learning. *Computers & Geosciences* 182, 105497.
- Song, Y., Wang, T., Cai, P., Mondal, S.K., Sahoo, J.P., 2023. A comprehensive survey of few-shot learning: Evolution, applications, challenges, and opportunities. *ACM Computing Surveys* 55, 1–40.
- Srivastava, R., Sen, M., 2009. Fractal-based stochastic inversion of poststack seismic data using very fast simulated annealing. *Journal of Geophysics and Engineering* 6, 412–425.
- Su, Y., Cao, D., Liu, S., Hou, Z., Feng, J., 2023. Seismic impedance inversion based on deep learning with geophysical constraints. *Geoenergy Science and Engineering* 225, 211671.
- Sun, H., Zhang, J., Xue, Y., Zhao, X., 2024. Seismic inversion based on fusion neural network for the joint estimation of acoustic impedance and porosity. *IEEE Transactions on Geoscience and Remote Sensing* .

- Tamaddon-Jahromi, H.R., Chakshu, N.K., Sazonov, I., Evans, L.M., Thomas, H., Nithiarasu, P., 2020. Data-driven inverse modelling through neural network (deep learning) and computational heat transfer. *Computer Methods in Applied Mechanics and Engineering* 369, 113217.
- Webb, T., Dulberg, Z., Frankland, S., Petrov, A., O'Reilly, R., Cohen, J., 2020. Learning representations that support extrapolation, in: *International conference on machine learning*, PMLR. pp. 10136–10146.
- Wu, B., Xie, Q., Wu, B., 2022. Seismic impedance inversion based on residual attention network. *IEEE Transactions on Geoscience and Remote Sensing* 60, 1–17.
- Wu, X., Liang, L., Shi, Y., Fomel, S., 2019. Faultseg3d: Using synthetic data sets to train an end-to-end convolutional neural network for 3d seismic fault segmentation. *Geophysics* 84, IM35–IM45.
- Wu, X., Yan, S., Bi, Z., Zhang, S., Si, H., 2021. Deep learning for multidimensional seismic impedance inversion. *Geophysics* 86, R735–R745.
- Xu, K., Zhang, M., Li, J., Du, S., Kawarabayashi, K., Jegelka, S., 2021. How neural networks extrapolate: From feedforward to graph neural networks, in: *International Conference on Learning Representations (ICLR)*.
- Yang, L., Chen, W., Wang, H., Chen, Y., 2021. Deep learning seismic random noise attenuation via improved residual convolutional neural network. *IEEE Transactions on Geoscience and Remote Sensing* 59, 7968–7981.
- Yuan, S., Jiao, X., Luo, Y., Sang, W., Wang, S., 2022. Double-scale supervised inversion with a data-driven forward model for low-frequency impedance recovery. *Geophysics* 87, R165–R181.
- Yuan, S., Wang, S., Luo, Y., Wei, W., Wang, G., 2019. Impedance inversion by using the low-frequency full-waveform inversion result as an a priori model. *Geophysics* 84, R149–R164.
- Zhang, B., Pu, Y., Dai, R., Cao, D., 2025. Seismic poststack impedance inversion using geophysics-informed deep-learning neural network. *Interpretation* 13, T219–T232.

- Zhang, G., Lin, C., Chen, Y., 2020. Convolutional neural networks for micro-seismic waveform classification and arrival picking. *Geophysics* 85, WA227–WA240.
- Zhang, H., Chen, T., Liu, Y., Zhang, Y., Liu, J., 2021. Automatic seismic facies interpretation using supervised deep learning. *Geophysics* 86, IM15–IM33.
- Zhao, L., Cao, D., Zhang, Y., An, Z., Lin, K., Wen, X., 2025. Alternate iterative inversion of acoustic impedance and wavelet based on sparse constraints. *IEEE Transactions on Geoscience and Remote Sensing* .
- Zhu, G., Chen, X., Li, J., Guo, K., 2022. Data-driven seismic impedance inversion based on multi-scale strategy. *Remote Sensing* 14, 6056.
- Zhu, X., Li, K., Yang, Z., Li, Z., 2025a. Swininver: 3d data-driven seismic impedance inversion based on swin transformer and adversarial training. *Computers & Geosciences* 194, 105743.
- Zhu, Z., Wang, Z., Feng, Y., Zheng, W., 2025b. Solution and application of two-dimensional seismic wavefield evolution based on physics-informed neural networks. *Engineering Applications of Artificial Intelligence* 150, 110652.